Liu Z, Lin Z, Tao L.

Mass, momentum and energy flux conservation for nonlinear wave-wave interaction.

Physics of Fluids **2016, 28(12), 127104.**

DOI link to article:

http://dx.doi.org/10.1063/1.4971252

Date deposited:

21/11/2016

Mass, momentum and energy flux conservation for nonlinear wave-wave interaction

Zhen Liu[1, a)] Zhiliang Lin[1, 2, b)] Longbin Tao[3, c)]

[1]*State Key Laboratory of Ocean Engineering, Shanghai Jiao Tong University, 800 Dongchuan Road, Shanghai 200240, China*

[2]*Collaborative Innovation Center for Advanced Ship and Deep-Sea Exploration (CISSE), Shanghai Jiao Tong University, 800 Dongchuan Road, Shanghai 200240, China*

[3]*School of Marine Science and Technology, Newcastle University, Armstrong Building, Newcastle upon Tyne NE1 7RU, United Kingdom*

A fully nonlinear solution for bi-chromatic progressive waves in water of finite depth in the framework of the homotopy analysis method (HAM) is derived. The bi-chromatic wave field is assumed to be obtained by the nonlinear interaction of two monochromatic wave trains that propagate independently in the same direction before encountering. The equations for the mass, momentum and energy fluxes based on the accurate high-order homotopy series solutions are obtained using a discrete integration and a Fourier series-based fitting. The conservation equations for the mean rates of the mass, momentum and energy fluxes before and after the interaction of the two nonlinear monochromatic wave trains are proposed to establish the relationship between the steady-state bi-chromatic wave field and the two nonlinear monochromatic wave trains. The parametric analysis on ε_1 and ε_2, representing the nonlinearity of the bi-chromatic wave field, is performed to obtain a sufficiently small

[a)] Electronic mail: liuzhen0829@sjtu.edu.cn

[b)] Electronic mail: linzhiliang@sjtu.edu.cn This author contributed equally with the first author to this work (co-first author).

[c)] Author to whom correspondence should be addressed. Electronic mail: longbin.tao@newcastle.ac.uk

standard deviation S_d, which is applied to describe the deviation from the conservation state ($S_d = 0$) in terms of the mean rates of the mass, momentum and energy fluxes before and after the interaction. It is demonstrated that very small standard deviation from the conservation state can be achieved. After the interaction, the amplitude of the primary wave with a lower circular frequency is found to decrease; while the one with a higher circular frequency is found to increase. Moreover, the highest horizontal velocity of the water particles underneath the largest wave crest, which is obtained by the nonlinear interaction between the two monochromatic waves, is found to be significantly higher than the linear superposition value of the corresponding velocity of the two monochromatic waves. The present study is helpful to enrich and deepen the understanding with insight to steady-state wave-wave interactions.

I. INTRODUCTION

Ocean surface waves are irregular and intuitively viewed as a superposition of many monochromatic wave components of different frequencies and amplitudes. Nonlinear interactions among these wave components are very important to resultant wave properties. During the past several decades, a considerable number of studies have been carried out to analyze nonlinear wave interaction theories. Phillips[1] and Longuet-Higgins[2] initially revealed the resonant phenomenon obtained from nonlinear interactions between two or three wave trains. It was pointed out that, under specific conditions, conspicuous energy transfer occurs from primary waves to a tertiary wave, produced via the third-order interaction. Pierson[3] derived an oscillatory third-order perturbation solution for two and three collinear interacting Stokes waves in deep water. However, Madsen and Fuhrman[8] pointed out that the dispersion

relation obtained by Pierson[3] was not based on consistent perturbation principles and thus is incorrect, and they further presented a new third-order solution for bi-chromatic bi-directional water waves in finite depth, extending the second-order in finite depth and third-order in infinite depth theories of steady bi-chromatic waves. Their solution includes explicit expressions for the surface elevation, the amplitude dispersion and the velocity potential. Dalzell[4] employed symbolic computation to extend the second-order wave-wave interaction theory from deep water to finite water depth. Ohyama *et al*.[5] obtained a fourth-order solution for nonlinear interactions among multiple directional wave trains by using a Stokes-type expansion method. It was indicated that the third- and fourth-order components may produce isolated large crests in random wave fields. Chen and Zhang[6] studied the interaction between a unidirectional deep-water short-wave train and an intermediate water-depth long wave using a conventional perturbation method and a phase modulation method, respectively. It was revealed that the modulation of the short-wave intrinsic frequency and potential amplitude along the long-wave surface become significant as water depth decreases, together with the increasing modulation of the short-wave phase, amplitude and wave number. Zhang and Chen[7] further derived a general third-order analytical solution for the strong interactions among three collinear free-wave components using a perturbation method, and this solution is regarded as the kernel of third-order collinear irregular wave theory.

Most of the aforementioned studies are based on the perturbation technique due to its solid mathematical foundation on the basis of the asymptotic expansion with respect to some small parameters. As the nonlinearity increases, in order to obtain accurate results, higher-order solutions are required. However, the derivation of the higher-order perturbation

66 solution for nonlinear wave-wave interaction problems can be lengthy and very complex.

67 Jang and Kwon[9] proposed a fixed point approach to calculate nonlinear monochromatic
68 wave profiles and later Jang *et al.*[10] apply to evaluate the nonlinear wave profiles of
69 wave-wave interactions in a finite water depth. It is worth noting that the results by Jang *et*
70 *al.*[10] do not satisfy the exact kinematic and dynamic free surface boundary conditions and
71 thus fail to capture strongly nonlinear features. To evaluate the strongly nonlinear
72 characteristics of wave-wave interaction, Lin *et al.*[11] investigated fully nonlinear bi-chromatic
73 unidirectional waves propagating in deep water using the so-called homotopy analysis
74 method (HAM). The particular advantage of HAM is its independent of small parameters and
75 suitable to solve strongly nonlinear problems. Other advantages associated with HAM
76 include a greater flexibility in the selection of a proper set of base functions for the solution
77 and a simple way in the control of the convergence rate and region of solution series (Liao[12]).

78 HAM was first applied to monochromatic, progressive waves in deep water by Liao and
79 Cheung[13]. Later, Tao et al.[14] successfully extended Liao and Cheung[13] to waters of finite
80 depth. More recently, Liao[15] proposed a multiple-variable technique to investigate
81 steady-state resonant progressive waves in deep water in the framework of HAM. It is
82 demonstrated that there exist multiple resonant waves, and that the amplitudes of resonant
83 wave may be much smaller than those of primary waves thus the resonant waves sometimes
84 contain fairly small part of wave energy. Xu *et al.*,[16] further confirmed the existence of
85 steady-state resonant progressive waves in finite water depth by means of HAM and obtained
86 qualitatively identical conclusion using the Zakharov equation. Liu and Liao[17] extended the
87 existing results of Liao[15] and Xu et al.[16] on steady-state resonance from a single special

quartet to more general and coupled resonant quartets, as well as a resonant sextet. The aforementioned studies on steady-state wave resonance are based on the assumption that all of the wave amplitudes, wave numbers and wave frequencies are independent of time in the wave system. To date, however, whether or not HAM can be applied to address the unsteady-state wave resonance involving complicated issues, which can account for the wave instability phenomena[18] (e.g. modulational instability, also known as Benjamin-Feir instability), deserves further investigation.

Most of the aforementioned studies were focused on the resultant wave field produced by the interaction between two or multiple progressive wave components. The relationship between the resultant wave field and the monochromatic progressive waves before the interaction has not yet been discussed. Neglecting viscous dissipation, Baddour and Song[19, 20] introduced conservation equations for the mean rates of the mass, momentum and energy fluxes before and after the interaction between collinear current-free monochromatic waves and a wave-free current based on a perturbation method. Zaman and Baddour[21] further extended the work by Baddour and Song[19, 20] to a three-dimensional flow frame. However, the interaction of two nonlinear monochromatic progressive wave components which propagate independently before encountering, in terms of the conservation equations for the mass, momentum and energy fluxes, has not been considered. In this paper, by including constant water depth in the solution procedure, the present study extends Lin *et al.*[11] from infinite water depth to finite water depth. Furthermore, based on the assumption that the steady-state bi-chromatic wave system can be obtained by the interaction of two nonlinear monochromatic progressive wave trains which propagate independently in the same direction

before encountering, the present study aims to establish the relationship between the steady bi-chromatic wave field and the two nonlinear monochromatic progressive wave trains, in terms of the conservation equations for the mean rates of the mass, momentum and energy fluxes before and after the interaction, respectively.

The present paper is organized as follows. The mathematical description of the bi-chromatic wave field is given in Sec. II following the introduction. The definitions of the equations for the mass, momentum and energy fluxes are introduced in Sec. III. The conservation equations for the wave-wave interaction are presented in Sec. IV. The detailed results on the parametric analysis for the standard deviation from the conservation state ($S_d = 0$), as well as the characteristics of the bi-chromatic wave field with sufficiently small values for S_d, which is defined to describe the deviation from the conservation state before and after interaction, are discussed in Sec. V. Finally, conclusions are given, with the detailed solution procedure based on HAM in Appendix.

II. MATHEMATICAL DESCRIPTION OF THE BI-CHROMATIC WAVE FIELD

A. Basic equations

Fig. 1 shows the definition sketch for a steady-state bi-chromatic wave field which is assumed to be produced by the interaction of two nonlinear, monochromatic, progressive wave components that propagate independently in the same direction before interacting. A Cartesian coordinate system (x, z) is adopted where the $x-$axis is positive in the direction of wave propagation, and the $z-$axis is positive vertically upwards from the still water level as shown in Fig. 1. It is assumed that the nonlinear monochromatic wave train with a higher phase velocity will catch up to and interact thoroughly with the one with a lower phase

velocity, yielding the steady-state bi-chromatic wave field. For the bi-chromatic wave field, the fluid considered is inviscid and incompressible, and the flow is assumed to be irrotational. The quantities $\varphi(x,z,t)$ and $\zeta(x,t)$ are defined as the velocity potential and the wave elevation, respectively. The fluid motion described by the velocity potential φ is governed by the Laplace equation:

$$\nabla^2\varphi(x,z,t)=0, \quad -\infty<x<+\infty,\ -d<z<\zeta(x,t), \tag{1}$$

and subject to two nonlinear free surface conditions:

$$\frac{\partial\zeta}{\partial t}+\frac{\partial\varphi}{\partial x}\frac{\partial\zeta}{\partial x}-\frac{\partial\varphi}{\partial z}=0, \quad z=\zeta(x,t), \tag{2}$$

$$g\zeta+\frac{1}{2}(\nabla\varphi)\cdot(\nabla\varphi)+\frac{\partial\varphi}{\partial t}=0, \quad z=\zeta(x,t), \tag{3}$$

and the following condition at the bottom:

$$\frac{\partial\varphi}{\partial z}=0, \quad z=-d, \tag{4}$$

where $\nabla=(\partial/\partial x,\ \partial/\partial z)$, t denotes time, g is gravitational acceleration and d is the water depth. Since gravity capillary waves caused by surface tension are quite small compared to their wavelengths, the effect of surface tension is neglected.

Combining Eqs. (2) and (3), the free surface boundary condition becomes

$$\frac{\partial^2\varphi}{\partial t^2}+g\frac{\partial\varphi}{\partial z}+\frac{\partial\left[(\nabla\varphi)\cdot(\nabla\varphi)\right]}{\partial t}+\frac{1}{2}(\nabla\varphi)\cdot\nabla\left[(\nabla\varphi)\cdot(\nabla\varphi)\right]=0, \quad z=\zeta(x,t). \tag{5}$$

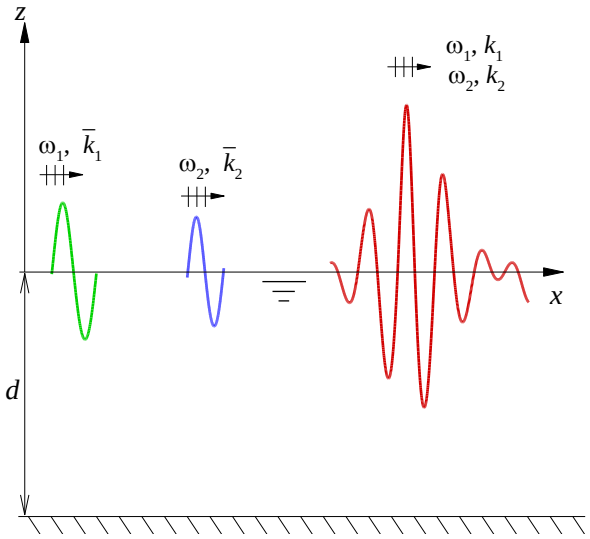

FIG. 1. Definition sketch for a steady-state bi-chromatic wave field.

B. Multiple-variable transformation

The frequencies and wave numbers of the primary waves of the bi-chromatic wave field are defined by ω_i and k_i ($i=1,2$), respectively. It is convenient to define the phase functions:

$$\theta_1 = k_1 x - \omega_1 t + \Phi_1, \tag{6}$$

$$\theta_2 = k_2 x - \omega_2 t + \Phi_2, \tag{7}$$

where Φ_i $(i=1,2)$ denotes an arbitrary, constant phase for zero time at the origin of the $x-z$ coordinate system. Whilst $k_1\omega_2 \neq k_2\omega_1$, the above two variables can be applied to replace the variables x and t, and then the time t will not appear explicitly for a steady-state wave system. Thus, the potential function and wave elevation for the steady-state bi-chromatic wave field can be expressed as $\varphi(x,z,t)=\phi(\theta_1,\theta_2,z)$ and $\zeta(x,t)=\eta(\theta_1,\theta_2)$, respectively. With these definitions, the governing equation becomes

$$\hat{\nabla}^2\phi = k_1^2\frac{\partial^2\phi}{\partial\theta_1^2} + 2k_1k_2\frac{\partial^2\phi}{\partial\theta_1\partial\theta_2} + k_2^2\frac{\partial^2\phi}{\partial\theta_2^2} + \frac{\partial^2\phi}{\partial z^2} = 0, \qquad -d < z < \eta(\theta_1,\theta_2), \tag{8}$$

which is subject to the bottom boundary condition:

$$\frac{\partial\phi}{\partial z} = 0, \qquad z = -d, \tag{9}$$

and the nonlinear free surface conditions:

$$\eta = \frac{1}{g}(\omega_1\frac{\partial\phi}{\partial\theta_1} + \omega_2\frac{\partial\phi}{\partial\theta_2} - f), \qquad z = \eta(\theta_1,\theta_2), \tag{10}$$

$$\begin{aligned}&\omega_1^2\frac{\partial^2\phi}{\partial\theta_1^2} + 2\omega_1\omega_2\frac{\partial^2\phi}{\partial\theta_1\partial\theta_2} + \omega_2^2\frac{\partial^2\phi}{\partial\theta_2^2} + g\frac{\partial\phi}{\partial z}\\ &-2(\omega_1\frac{\partial f}{\partial\theta_1} + \omega_2\frac{\partial f}{\partial\theta_2}) + \hat{\nabla}\phi\cdot\hat{\nabla}f = 0, \qquad z = \eta(\theta_1,\theta_2),\end{aligned} \tag{11}$$

where

$$f = \frac{1}{2}\left[k_1^2(\frac{\partial\phi}{\partial\theta_1})^2 + 2k_1k_2\frac{\partial\phi}{\partial\theta_1}\frac{\partial\phi}{\partial\theta_2} + k_2^2(\frac{\partial\phi}{\partial\theta_2})^2 + (\frac{\partial\phi}{\partial z})^2\right], \tag{12}$$

and

$$\hat{\nabla} = (k_1\partial/\partial\theta_1 + k_2\partial/\partial\theta_2,\ \partial/\partial z). \tag{13}$$

Due to the nonlinear interaction, the wave elevation should be in the form:

$$\eta(\theta_1,\theta_2) = \sum_{m=0}^{+\infty}\sum_{n=-\infty}^{+\infty} a_{m,n}\cos(m\theta_1 + n\theta_2), \tag{14}$$

and the corresponding potential function should be in the form:

$$\phi(\theta_1,\theta_2,z) = \sum_{m=0}^{+\infty}\sum_{n=-\infty}^{+\infty} b_{m,n}\Psi_{m,n}(\theta_1,\theta_2,z), \tag{15}$$

where

$$\Psi_{m,n}(\theta_1,\theta_2,z) = \sin(m\theta_1 + n\theta_2)\frac{\cosh\left[|mk_1 + nk_2|(z+d)\right]}{\cosh\left[|mk_1 + nk_2|d\right]}, \tag{16}$$

and $a_{m,n}$, $b_{m,n}$ are constants to be determined. It should be noted that (15) automatically satisfies the governing Eq. (8) and the bottom boundary condition (9).

C. Solution procedures

As a first step to consider the nonlinear effects on the steady-state bi-chromatic waves in finite water depth, it is assumed that the nonlinear dispersion relation in the wave system can

be described as $\omega_i = \varepsilon_i \sqrt{g k_i \tanh(k_i d)}$ $(i = 1,2)$, where ε_i is a parameter slightly larger than 1, representing the nonlinearity of the wave system. As long as ε_i, ω_i, and d are given, k_i can be easily obtained by the nonlinear dispersion relation. Once ω_i, k_i and d are known, it is not difficult to obtain $a_{m,n}$ and $b_{m,n}$ by HAM.

Lin *et al.*[11] successfully applied HAM to obtain a high-order series solution for deep-water bi-chromatic progressive waves. The effectiveness of HAM for wave-wave interaction was validated by Lin *et al.*[11] by comparing the HAM solutions for the wave profile and water particle velocity with those obtained based on the perturbation technique. For the sake of simplicity, a brief description of the solution procedure in the framework of HAM is provided in Appendix. It is worth noting that the HAM solution procedure for each nonlinear monochromatic wave train is similar to that for the bi-chromatic waves, and the detailed HAM solution procedure for monochromatic, progressive waves can also be found in Liao and Cheung[13] and Tao *et al.*[14]

Validation of the analytical model

The present analytical model for bi-chromatic progressive waves in finite water depth is validated by comparison to experimental data of Ma et al.[22] Table I shows the parameters of the bi-chromatic wave cases in the experiments of Ma et al.[22] and corresponding results obtained by HAM. As shown in Table I, for the identical frequencies (f_1 and f_2) of primary waves of each case (Cases1-4) in the experiments and HAM solutions, the amplitudes of primary waves ($a_{1,0}$ and $a_{0,1}$) obtained by HAM have slight differences with those (a_1 and a_2) in the experiments, respectively. This is attributed to the nonlinear characteristics of the HAM solution. Moreover, the total averaged residual square error (E_m^T) of Cases1-4 holds a

fairly small value, which reaches at least the order of magnitude of 10^{-4}. This indicates that the HAM solution for Cases 1-4 possesses higher accuracy. Fig. 2 shows the time series of wave elevation for Case 1-4 by the HAM solution, together with the experimental data by Ma et al.[22] and corresponding linear superposition results. It can be clearly seen in Fig. 2 that, in comparison to the linear superposition results, the HAM solution demonstrates a much better agreement with the experimental data. This further verifies the effectiveness of the present analytical model.

TABLE I. Parameters of bi-chromatic waves ($d = 0.5$ m)

Case	Exp. (Ma et al.[22]) & HAM		Exp.(Ma et al.[22])		HAM		E_m^T (m=10)
	f_1 (Hz)	f_2 (Hz)	a_1 (m)	a_2 (m)	$a_{1,0}$ (m)	$a_{0,1}$ (m)	
1	0.9	1.1	0.0185	0.0205	0.018541	0.020487	1.15E-08
2	0.875	1.125	0.0185	0.0205	0.018526	0.021357	1.31E-07
3	0.85	1.15	0.0185	0.0205	0.018452	0.021344	3.64E-06
4	0.825	1.175	0.0185	0.0205	0.018555	0.026647	1.30E-04

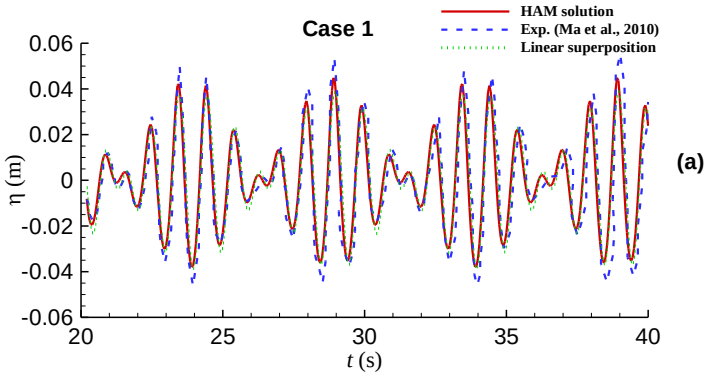

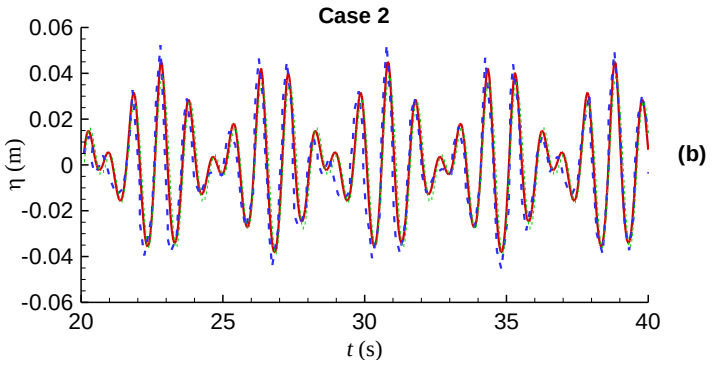

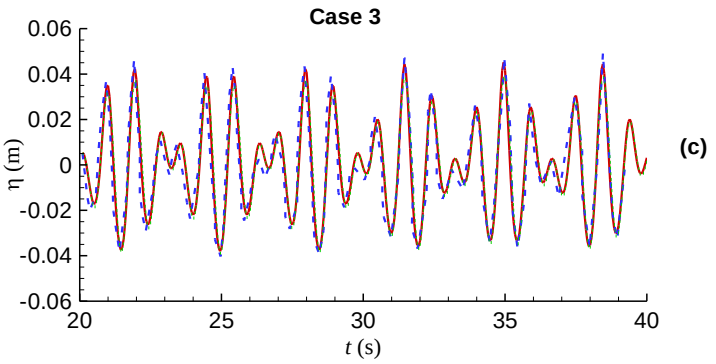

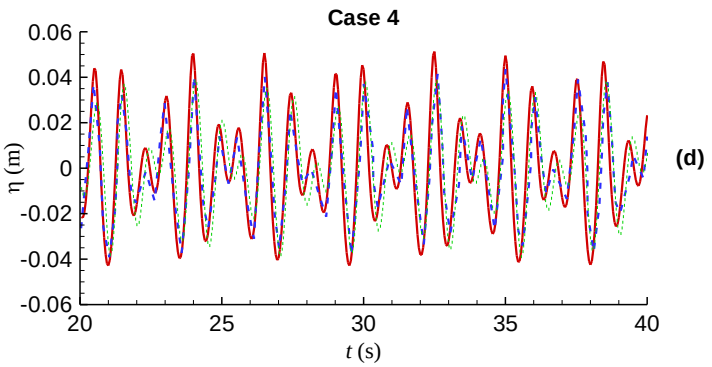

FIG. 2. Comparisons of time series of wave elevation between the HAM solutions, the experimental data and corresponding linear superposition results

Lin et al.[11] compared the nonlinear amplitude dispersion for bi-chromatic unidirectional waves in deep water obtained by HAM to the 3rd-order perturbation results by Madsen and Fuhrman[8]. It is demonstrated that, for the bi-chromatic waves with identical amplitude ($a_{1,0} = a_{0,1}$) of the two primary wave components and different wave numbers (k_1, k_2)=(0.3, 0.4), the HAM solutions agree well with the perturbation results when $k_1 a_{1,0} < 0.045$ (or

226 $k_2 a_{0,1} < 0.06$), and exhibit a relatively evident misalignment with the perturbation results
227 when $k_1 a_{1,0} > 0.045$. In this paper, to further validate the effectiveness of the present
228 analytical model, the nonlinear amplitude dispersions for interacting bi-chromatic
229 unidirectional waves in finite water depth by HAM are compared to those by Madsen and
230 Fuhrman[8]. Table II shows the parameters for the study of nonlinear amplitude dispersion. The
231 wave numbers of each case of Table II in the HAM solution and the perturbation solution are
232 (k_1, k_2)=(0.2, 0.285714). The amplitudes of primary waves ($a_{1,0}$ and $a_{0,1}$) of each case in
233 the HAM solution and the perturbation solution are increasing gradually from Case A1 to
234 A10, respectively, indicating the nonlinearity of the bi-chromatic wave system is stronger and
235 stronger. It is noted that the relative water depths of the two primary wave components are
236 $k_1 d = 2$ and $k_2 d = 2.86$, respectively, corresponding to intermediate depth wave conditions.
237 As shown in Table II, the values for the relative nonlinear frequencies $\omega_1 / \bar{\omega}_1$ and $\omega_2 / \bar{\omega}_2$
238 obtained by HAM agree well with the 3rd-order perturbation results from Cases A1 to A5, and
239 have relatively large differences from Case A6 to A10.

240 To clearly see the tendency of the nonlinear amplitude dispersion, $\omega_1 / \bar{\omega}_1$ and $\omega_2 / \bar{\omega}_2$
241 are plotted against $a_{1,0}$ and $a_{0,1}$ in Fig. 3, respectively. It can be evidently seen that the
242 HAM solution appears to be different with the perturbation results starting from Case A6
243 ($a_{1,0} = 0.202365$, $a_{0,1} = 0.42256$). The total averaged residual square error for Cases A6-A10
244 reaches at least the order of magnitude of 10^{-5}, indicating that the present HAM solutions
245 are highly accurate. To further demonstrate the convergence of the HAM solution, Fig. 4
246 shows the total averaged residual square error E_m^T versus m with $c_0 = -1$ in Case A10. It
247 can be seen that even for this relatively strongly nonlinear case (A10), E_m^T decreases

248 gradually to the order of magnitude of 10^{-6} as m increases from 1 to 20. This means that

249 the HAM solution for this case is convergent.

250 TABLE II. Parameters for the study of nonlinear amplitude dispersion ($k_1 d = 2,\ k_2 d = 2.86$)

Case	$a_{1,0}$ (m)	$a_{0,1}$ (m)	3rd-order perturbation (Madsen & Fuhrman[8])		HAM		E_m^T (m=10)
			$\omega_1 / \bar{\omega}_1$	$\omega_2 / \bar{\omega}_2$	$\omega_1 / \bar{\omega}_1$	$\omega_2 / \bar{\omega}_2$	
A1	0.052989	0.14654	1.001	1.00101	1.001	1.001	1.42E-07
A2	0.07738	0.205276	1.00198	1.00201	1.002	1.002	2.08E-07
A3	0.115589	0.284759	1.00384	1.00394	1.004	1.004	2.14E-07
A4	0.14787	0.34188	1.00559	1.00579	1.006	1.006	1.86E-07
A5	0.176573	0.386578	1.00722	1.00755	1.008	1.008	8.32E-07
A6	0.202365	0.42256	1.00871	1.00918	1.01	1.01	8.36E-07
A7	0.224841	0.451334	1.01002	1.01064	1.012	1.012	6.09E-07
A8	0.244576	0.473958	1.01114	1.01191	1.014	1.014	8.22E-07
A9	0.261417	0.490857	1.01204	1.01296	1.016	1.016	9.12E-06
A10	0.275165	0.502195	1.01269	1.01375	1.018	1.018	7.25E-05

251

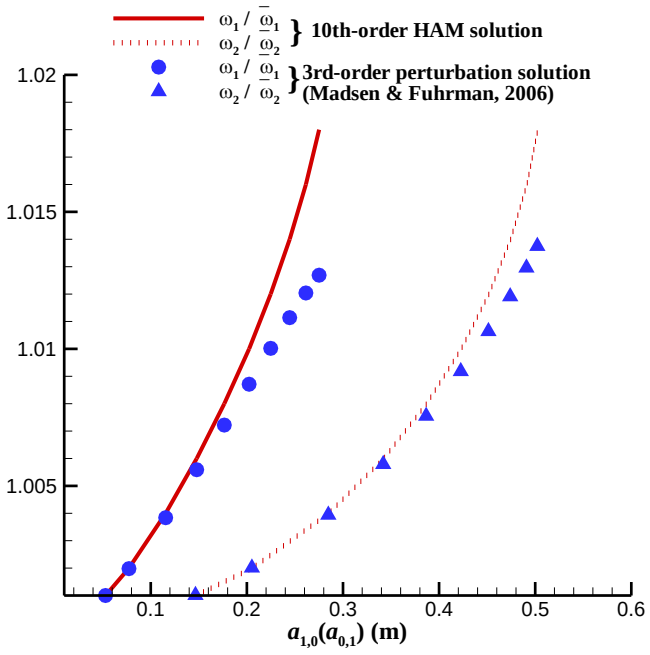

252

253 FIG. 3. Comparison of nonlinear amplitude dispersion between HAM solutions and

254 perturbation results by Madsen and Fuhrman[8]

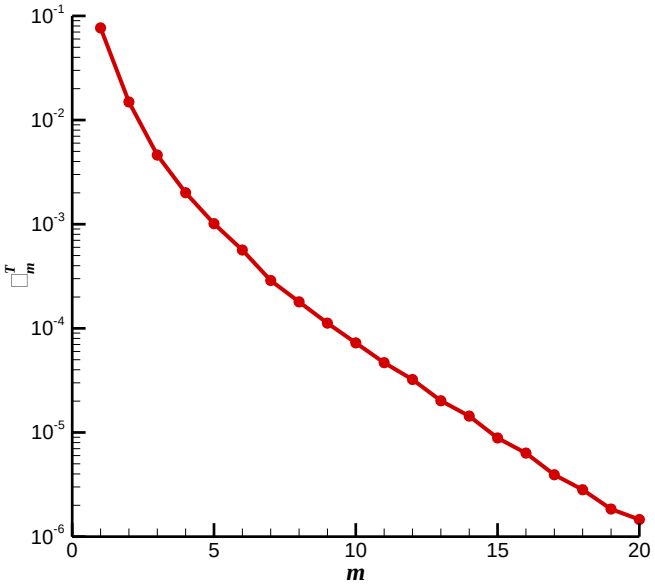

255

256 FIG. 4. The total averaged residual square error E_m^T versus m with $c_0 = -1$ in Case A10

257

258 ## III. DEFINITION OF MASS, MOMENTUM AND ENERGY FLUX EQUATIONS

259 Similar to the flux equations in Whitham[23], the mean rates of the mass, momentum and

260 energy fluxes across a vertical section fixed in the bi-chromatic wave field, denoted by Q^{BW},

261 M^{BW}, and E^{BW} respectively, can be written as

262 $$Q^{BW} = \frac{1}{4\pi^2}\int_0^{2\pi}\int_0^{2\pi}\int_{-d}^{\eta}\rho\phi_x \,\mathrm{d}z\,\mathrm{d}\theta_1\,\mathrm{d}\theta_2, \tag{17}$$

263 $$M^{BW} = \frac{1}{4\pi^2}\int_0^{2\pi}\int_0^{2\pi}\int_{-d}^{\eta}(P+\rho\phi_x^2)\,\mathrm{d}z\,\mathrm{d}\theta_1\,\mathrm{d}\theta_2, \tag{18}$$

264 $$E^{BW} = \frac{1}{4\pi^2}\int_0^{2\pi}\int_0^{2\pi}\int_{-d}^{\eta}\left[P+\frac{\rho}{2}(\phi_x^2+\phi_z^2)+\rho g z\right]\phi_x \,\mathrm{d}z\,\mathrm{d}\theta_1\,\mathrm{d}\theta_2, \tag{19}$$

265 where ρ denotes density of water, and P is the total pressure which can be determined by

266 the Bernoulli equation for the wave field as

267 $$\frac{P}{\rho} = -\frac{\partial\phi}{\partial t} - \frac{1}{2}(\nabla\phi)^2 - gz. \tag{20}$$

268 Different from the method for computing the integral quantities of the mass, momentum and

269 energy fluxes by means of low-order perturbation approximations by Whitham[23], Baddour

and Song[19, 20] and Zaman and Baddour[21], the accurate high-order homotopy series solutions for the pressure, water particle velocity and free surface elevation are employed to calculate the corresponding integrations for the present bi-chromatic wave cases, i.e. Q^{BW}, M^{BW} and E^{BW}. Due to the complex integrands and integral upper limit incorporating the variable x and t, it is difficult to obtain these integral quantities by direct integrating. Thus, the phase function $\theta_i = k_i x - \omega_i t \quad (i = 1, 2)$ is applied to instead of x and t in the integrands and integral upper limit to carry out the discrete integration as illustrated below. Then, the obtained discrete integral data points are fitted using the double Fourier series. The functions obtained by fitting can be deemed as the corresponding integral expressions for the mass, momentum and energy fluxes, respectively. The discrete integration can be described as

$$QD_{i,j}^{BW} = \int_{-d}^{\eta_{i,j}} \rho \phi_x(\theta_1, \theta_2, z)\Big|_{\theta_1 = i\Delta\theta_1, \theta_2 = j\Delta\theta_2} \mathrm{d}z, \tag{21}$$

$$MD_{i,j}^{BW} = \int_{-d}^{\eta_{i,j}} [P(\theta_1, \theta_2, z) + \rho {\phi_x}^2(\theta_1, \theta_2, z)]\Big|_{\theta_1 = i\Delta\theta_1, \theta_2 = j\Delta\theta_2} \mathrm{d}z, \tag{22}$$

$$ED_{i,j}^{BW} = \int_{-d}^{\eta_{i,j}} \left\{ P(\theta_1, \theta_2, z) + \frac{\rho}{2}[{\phi_x}^2(\theta_1, \theta_2, z) + {\phi_z}^2(\theta_1, \theta_2, z)] + \rho g z \right\} \phi_x(\theta_1, \theta_2, z)\Big|_{\theta_1 = i\Delta\theta_1, \theta_2 = j\Delta\theta_2} \mathrm{d}z, \tag{23}$$

where $\eta_{i,j} = \eta(\theta_1, \theta_2)\big|_{\theta_1 = i\Delta\theta_1, \theta_2 = j\Delta\theta_2}$, $i = 0, 1, \cdots, I$, $j = 0, 1, \cdots, J$, I and J are the numbers of the discrete points, $\Delta\theta_1 = 4\pi / I$ and $\Delta\theta_2 = 4\pi / J$. In the present work, the discrete integrations are calculated with $I = J = 20$ to obtain sufficient integral data points for the subsequent fitting. It is worth noting that all the integral quantity expressions for each nonlinear monochromatic wave field based on the HAM solution are similar to those for the bi-chromatic wave field.

To illustrate the calculation and fitting procedure for the discrete integration, consider the bi-chromatic wave case with $\varepsilon_1 = \varepsilon_2 = 1.008$. As shown in Fig. 5(a-c), the filled circles representing the integral values are obtained by using the above discrete integration. The

double Fourier series $F(\theta_1,\theta_2)=\sum_{h=0}^{N}\sum_{l=-N}^{N} f_{h,l}\cos(h\theta_1+l\theta_2)$ is employed to fit the discrete integral data points to obtain the continuous functions for the mass, momentum and energy fluxes, which are represented by $F_Q(\theta_1,\theta_2)$, $F_M(\theta_1,\theta_2)$ and $F_E(\theta_1,\theta_2)$, respectively. Taking $N=4$, the Fourier coefficients $f_{h,l}$ for the fitted functions for the mass, momentum and energy fluxes of the bi-chromatic wave case with $\varepsilon_1=\varepsilon_2=1.008$ were obtained, and shown in Table III-V, respectively. As clearly shown in Fig. 5(a-c), the curves for the fitted functions agree well with the discrete integral value points, indicating that the corresponding integral quantities can be represented by the fitted functions based on the double Fourier series. Thus, the mean rates of the mass, momentum and energy fluxes across a vertical section fixed in the bi-chromatic wave field can be obtained as

$$Q_F^{BW}=\frac{1}{4\pi^2}\int_0^{2\pi}\int_0^{2\pi}F_Q(\theta_1,\theta_2)\,\mathrm{d}\theta_1\,\mathrm{d}\theta_2, \tag{24}$$

$$M_F^{BW}=\frac{1}{4\pi^2}\int_0^{2\pi}\int_0^{2\pi}F_M(\theta_1,\theta_2)\,\mathrm{d}\theta_1\,\mathrm{d}\theta_2, \tag{25}$$

$$E_F^{BW}=\frac{1}{4\pi^2}\int_0^{2\pi}\int_0^{2\pi}F_E(\theta_1,\theta_2)\,\mathrm{d}\theta_1\,\mathrm{d}\theta_2. \tag{26}$$

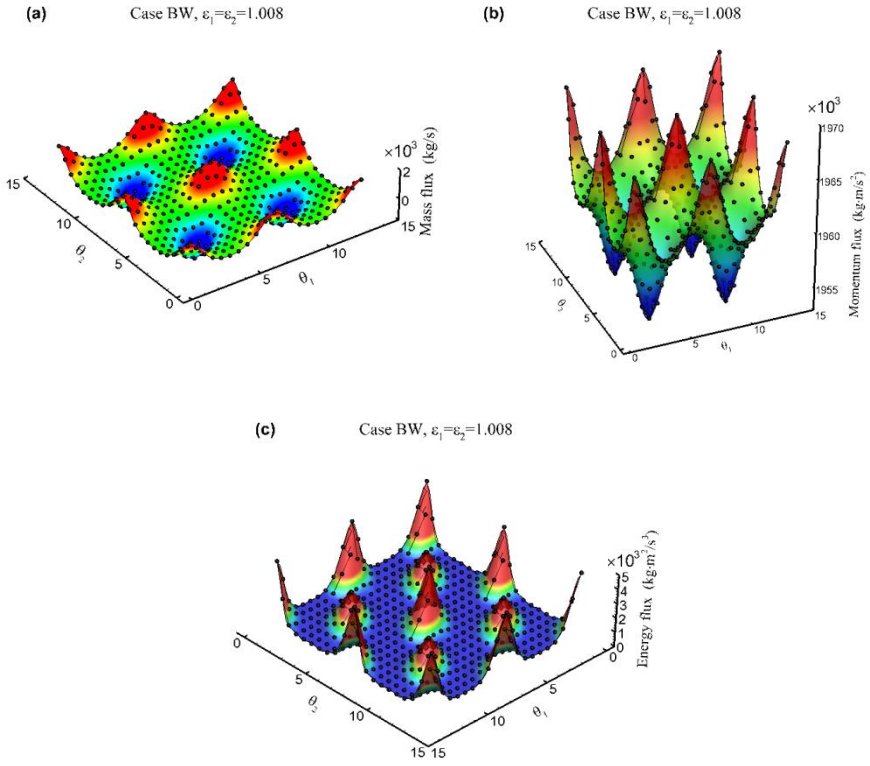

309

310

311 FIG. 5. The comparison of the discrete integral value points and fitted function curved

312 surfaces for : (a) Mass flux; (b) Momentum flux; (c) Energy flux (Filled circle: the discrete

313 integrations; curved surface: the fitted functions) of the Case BW with $\varepsilon_1 = \varepsilon_2 = 1.008$.

314

315 TABLE III. The coefficients for the fitted function $F_Q(\theta_1, \theta_2)$ for the mass flux of the Case

316 BW with $\varepsilon_1 = \varepsilon_2 = 1.008$

$f_{h,l}$		h				
		0	1	2	3	4
l	-4	0.000397	0.00381422	0.013113	0.0230707	-0.00125484
	-3	0.002415	0.0260936	0.0674599	-0.00109471	-0.000143365
	-2	0.021295	0.231307	-0.00160349	0.00763481	0.00100312
	-1	0.349504	-0.00320619	0.0851259	0.00393892	0.000593725
	0	0.0438276	0.56839	0.0182248	0.00127507	0.000381219
	1	0.349504	0.0400968	0.00288494	0.000442871	0.000326527
	2	0.021295	0.0045469	0.000559225	0.000288311	0.000386793
	3	0.002415	0.000731839	0.000245947	0.000423822	0.000788489
	4	0.000397	0.000257311	0.000498968	0.00137073	0.00249853

TABLE IV. The coefficients for the fitted function $F_M(\theta_1,\theta_2)$ for the momentum flux of the Case BW with $\varepsilon_1=\varepsilon_2=1.008$

$f_{h,l}$		h				
		0	1	2	3	4
l	-4	0.001678	0.0161032	0.0535568	0.0849963	-0.00285966
	-3	0.010824	0.112297	0.261621	-0.00223916	-0.00524012
	-2	0.096077	0.956645	-0.00322221	0.0577247	0.00451714
	-1	1.569255	-0.00663598	0.502256	0.0219407	0.00213071
	0	1960.1	2.85307	0.0922511	0.00637314	0.000879331
	1	1.569255	0.189722	0.0139074	0.00204607	0.000588102
	2	0.096077	0.0212458	0.00261023	0.00131989	0.000979566
	3	0.010824	0.0327857	0.00115836	0.00206073	0.00293329
	4	0.001678	0.00115417	0.00231043	0.00615209	0.0100231

TABLE V. The coefficients for the fitted function $F_E(\theta_1,\theta_2)$ for the energy flux of the Case BW with $\varepsilon_1=\varepsilon_2=1.008$

$f_{h,l}$		h				
		0	1	2	3	4
l	-4	0.005637	0.0473759	0.115674	0.0317512	0.031869
	-3	0.032586	0.247497	0.0676816	0.0948591	0.00947649
	-2	0.218464	0.125411	0.27686	0.0293963	0.0108733
	-1	0.087544	0.682447	0.0771108	0.0567149	0.00618863
	0	0.477811	0.150311	0.230699	0.0198214	0.00241005
	1	0.087544	0.450797	0.0443137	0.00606873	0.00138997
	2	0.218464	0.0658464	0.00897634	0.0034472	0.00251918
	3	0.032586	0.0112076	0.00379449	0.00557512	0.00764964
	4	0.005637	0.00397214	0.00731952	0.016681	0.0195476

IV. CONSERVATION EQUATIONS

Baddour and Song[19, 20] proposed the conservation equations based on linear and the second-order perturbation solutions in terms of the mean rates of the mass, momentum and

energy fluxes of a 2D current-free wave field, a wave-free uniform current field and a coexisting wave-current field. In their work, the wavelength, wave height, current velocity and water depth in the combined wave-current field were obtained based on the conservation equations for the mean rates of the mass, momentum and energy fluxes. Zaman and Baddour[21] further extended Baddour and Song[19, 20] to a 3D wave-current field in the framework of linear wave theory.

Without loss of generality, consider two 2D, weakly nonlinear, monochromatic wave trains propagating independently in the same direction before encountering. Table VI presents the parameters of the two nonlinear monochromatic wave trains, i.e. Cases W1 and W2, respectively, where $\varepsilon = \omega_i / \sqrt{g\bar{k}_i \tanh(\bar{k}_i d)}$; ω_i and $\bar{k}_i$ $(i = 1, 2)$ are the circular frequency and wave number of the corresponding monochromatic waves, respectively, as shown in Fig. 1. It is worth noting that, as pointed out by Liao and Cheung[13] and Tao et al.[14], HAM is suitable for strongly nonlinear monochromatic progressive waves in both deep and finite water depth whose wave steepness can approach up to the corresponding limiting value determined by the equation $(H / L)_{\max} = 0.142 \tanh(kd)$, in which H denotes wave height, L wavelength, k wave number and d water depth. However, in this work, the choosing criterion of the nonlinear parameter (ε) for Cases W1 and W2 depends on that the HAM solution for the bi-chromatic waves obtained by the interaction of the monochromatic wave Case W1 and W2 is convergent and has higher accuracy. That is why weakly nonlinear parameters are chosen for Case W1 and W2 as shown in Table VI. All the HAM solutions for Cases W1 and W2 are obtained with a total averaged residual error at least 10^{-6}, which is defined in Appendix and used to describe the accuracy of the homotopy series solution. Fig. 6

shows the wave profiles for Cases W1 and W2 at $t = 0$. Fig. 7 shows the comparison of the discrete integral value points and the fitted function curves for the mass, momentum and energy fluxes for Cases W1 and W2, respectively. It is clearly seen that the curves for the fitted functions agree well with the corresponding discrete integral value points. By means of the obtained fitted functions, the mean rates of the mass, momentum and energy fluxes across a fixed section, which are denoted by Q_F^{W1}, M_F^{W1} and E_F^{W1} for Case W1 and by Q_F^{W2}, M_F^{W2} and E_F^{W2} for Case W2 respectively, are calculated and presented in Table VII. The conservation equations for wave-wave interaction can be summarized as

$$Q_F^{W1} + Q_F^{W2} = Q_F^{BW}, \tag{27}$$

$$M_F^{W1} + M_F^{W2} = M_F^{BW}, \tag{28}$$

$$E_F^{W1} + E_F^{W2} = E_F^{BW}. \tag{29}$$

It is noted that the approximate solutions for the conservation equations of the mass, momentum and energy fluxes were obtained by Baddour and Song[19, 20] based on the low-order perturbation solutions for the current-free wave field and combined wave-current field. Due to the nonlinear feature of the interaction process, it is difficult to obtain the exact solutions for the bi-chromatic wave field, which is obtained via the interaction of the two nonlinear monochromatic wave trains, by solving the conservation Eqs (27)-(29). Thus, in this study, the standard deviation:

$$S_d = \sqrt{\frac{(r_Q - 1)^2 + (r_M - 1)^2 + (r_E - 1)^2}{3}} \tag{30}$$

is defined to illustrate the deviation from the conservation state ($S_d = 0$) of the mean rates of the mass, momentum and energy fluxes before and after the interaction of the two nonlinear monochromatic wave trains, where

372 $$r_Q = \frac{Q_F^{BW}}{Q_F^{W1} + Q_F^{W2}}, \quad r_M = \frac{M_F^{BW}}{M_F^{W1} + M_F^{W2}}, \quad r_E = \frac{E_F^{BW}}{E_F^{W1} + E_F^{W2}}. \tag{31}$$

373 Using the standard deviation S_d, it is not difficult to obtain a state evaluating the deviation

374 from the conservation state after the interaction of the two monochromatic wave trains.

375 TABLE VI. The monochromatic wave parameters ($d = 20$ m)

Case	ε	Circular frequency (rad/s)	Wave number (rad/m)	Wavelength (m)	Phase velocity (m/s)	Amplitude of primary waves (m)
W1	1.002	1.98386	0.4	15.708	4.96	0.157823
W2	1.002	2.21802	0.5	12.5664	4.44	0.126214

376

377

378

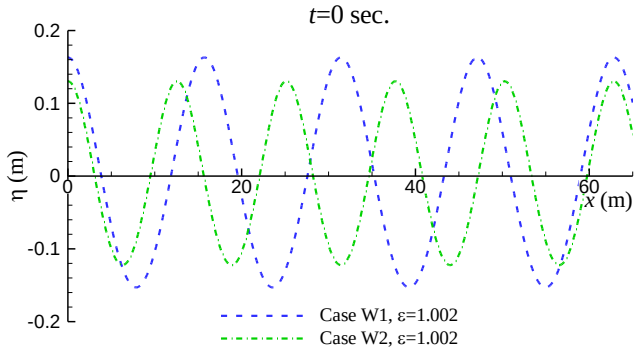

379

380 FIG. 6. Wave profile comparison for Cases W1 and W2

381

382

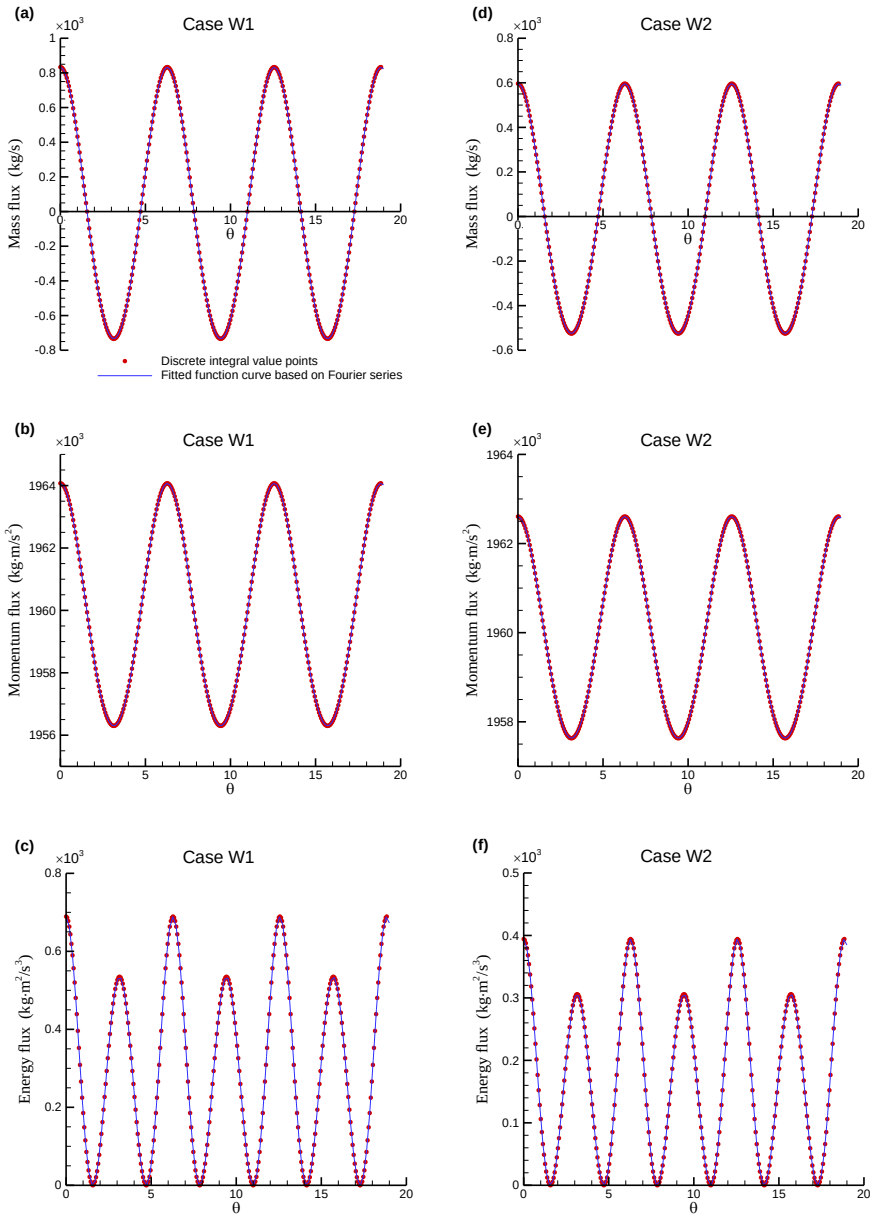

FIG. 7. The comparison of the discrete integral value points and fitted function curves for (a) and (d): Mass flux; (b) and (e): Momentum flux; (c) and (f): Energy flux of Cases W1 and W2.

TABLE VII. The mean rates of the mass, momentum and energy flux of Cases W1 and W2

Case	Mass flux (kg/s)	Momentum flux ($kg \cdot m/s^2$)	Energy flux ($kg \cdot m^2/s^3$)
W1	0.0246829×10^3	1960.06×10^3	0.304792×10^3

W2	0.0176491×10^{3}	1960.04×10^{3}	0.174348×10^{3}

V. RESULTS AND DISCUSSION

A. Analyses based on $\varepsilon_1=\varepsilon_2$

It is assumed that the nonlinear monochromatic wave Case W1 with a higher phase velocity (4.96 m/s) will catch up to the Case W2 with a lower phase velocity (4.44 m/s) and interact thoroughly, which results in the formation of a steady-state bi-chromatic wave field. The frequencies of the primary waves and water depth are assumed to be invariant before and after the interaction. As abovementioned, it is quite difficult to obtain the exact solutions for the conservation equations due to the nonlinear feature. The practice of this paper is to search the solutions for the conservation equations, which are applied to assess the deviation S_d from the conservation state ($S_d=0$). Firstly, a set of $\varepsilon_1(=\varepsilon_2)$ for the bi-chromatic wave field are utilized to investigate the deviation from the conservation state by means of the standard deviation S_d. Table VIII shows the bi-chromatic wave parameters for the conservation study. For the bi-chromatic wave field, for simplicity, it is easy to assume that $\varepsilon_1=\varepsilon_2$ with the same value (1.002) as that of the nonlinear monochromatic wave fields. As shown in Table VIII, for $\varepsilon_1=\varepsilon_2=1.002$, $S_d=0.555$ can be obtained based on the HAM solutions. However, for $\varepsilon_1=\varepsilon_2=1.001$, S_d tends to approach a much higher value (0.682). This indicates that a smaller value for $\varepsilon_1(=\varepsilon_2)$ leads to a larger discrepancy between the mean rates of the mass, momentum and energy fluxes before and after the interaction. For $\varepsilon_1(=\varepsilon_2)$ from 1.003 to 1.01 with an increment of 0.001, S_d approaches a relatively smaller value (0.013) at $\varepsilon_1=\varepsilon_2=1.008$, indicating that the case ($\varepsilon_1=\varepsilon_2=1.008$) is much closer to the conservation state

412 of the mass, momentum and energy fluxes than other cases in Table VIII.

413 TABLE VIII. The bi-chromatic wave parameters in the case of $\varepsilon_1 = \varepsilon_2$ ($d = 20$ m)

ε_1	ε_2	ω_1 (rad/s)	ω_2 (rad/s)	S_d	L_1(m)	L_2(m)	$a_{1,0}$(m)	$a_{0,1}$(m)
1.001	1.001	1.98386	2.21802	0.682	15.6766	12.5413	0.0487901	0.0660159
1.002	1.002	1.98386	2.21802	0.555	15.7079	12.5664	0.0678623	0.0918262
1.003	1.003	1.98386	2.21802	0.436	15.7393	12.5915	0.0814162	0.11022
1.004	1.004	1.98386	2.21802	0.327	15.7707	12.6166	0.0917175	0.124255
1.005	1.005	1.98386	2.21802	0.229	15.8021	12.6417	0.0996403	0.135117
1.006	1.006	1.98386	2.21802	0.140	15.8336	12.6669	0.105687	0.143485
1.007	1.007	1.98386	2.21802	0.061	15.8651	12.6921	0.110286	0.149906
1.008	1.008	1.98386	2.21802	0.013	15.8966	12.7173	0.113925	0.154952
1.009	1.009	1.98386	2.21802	0.082	15.9282	12.7426	0.117177	0.159348
1.01	1.01	1.98386	2.21802	0.157	15.9598	12.7679	0.120801	0.164024

414

415

416 Fig. 8 shows the wave profile comparison for the Cases BW with $\varepsilon_1 = \varepsilon_2 = 1.006$, 1.008
417 and 1.01 at $t = 0$. It can be clearly seen that the largest wave crest at $x = 0$ becomes higher
418 and higher as $\varepsilon_1 (= \varepsilon_2)$ increases, whilst the largest wave trough next to $x = 0$ becomes
419 lower and lower. This means that the largest wave height in the wave profile tends to increase
420 notably as ε_1 increases, although the increment in ε_1 is very small. However, the profiles
421 of the wave crest and trough around $x = 30$ (m) appear to be invariant.

422

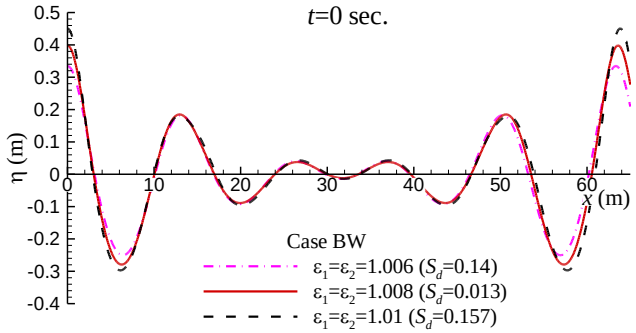

FIG. 8. Wave profile comparison between the Cases BW with $\varepsilon_1 = \varepsilon_2 = 1.006$, 1.008 and 1.01.

To investigate the frequency content of the bi-chromatic wave system, the time series of the wave elevation obtained from the HAM solutions are analyzed by FFT. Fig. 9(a-c) shows the amplitude spectra of the bi-chromatic wave system with $\varepsilon_1 = \varepsilon_2 = 1.006$, 1.008 and 1.01. As shown in Fig. 9(a-c), two dominant large amplitudes (at $f_1 \approx 0.314367$ Hz and $f_2 \approx 0.352342$ Hz) can be clearly seen and high-order nonlinear components of each bi-chromatic wave case are rather prominent. As $\varepsilon_1 (= \varepsilon_2)$ increases from 1.006 to 1.01, the nonlinearity becomes stronger and stronger and some higher-order wave components, e.g. the third order ($3f_1, 3f_2$, etc), become increasingly significant. Table IX presents the amplitudes of the wave components from the first order to the third order of the Cases BW with $\varepsilon_1 = \varepsilon_2 = 1.006$, 1.008 and 1.01, respectively. It can be clearly observed that the amplitudes of the wave components from the first order to the third order between these cases have remarkable difference. For example, the value for $a(f_1)$ in the case of $\varepsilon_1 = \varepsilon_2 = 1.008$ ($S_d = 0.013$) is 0.113925 m which is 7.5% greater than 0.105687 m in the case of $\varepsilon_1 = \varepsilon_2 = 1.006$ ($S_d = 0.140$), and 6.1% less than 0.120801 m in the case of $\varepsilon_1 = \varepsilon_2 = 1.01$ ($S_d = 0.157$). In fact, these different amplitudes indeed lead to the difference of the mean rates

of the mass, momentum and energy fluxes between these three cases, which can be assessed by the standard deviation (S_d) values from the conservation state.

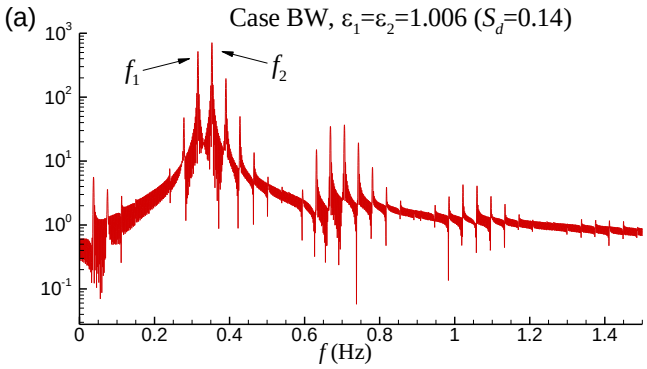

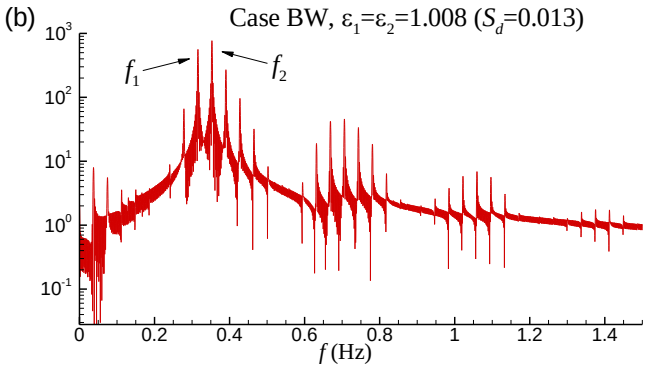

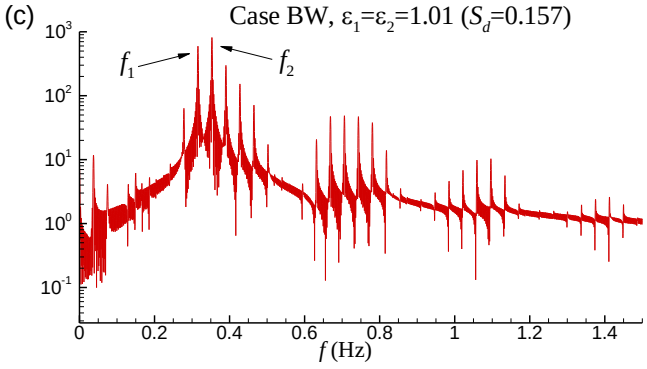

FIG. 9. Amplitude spectra for the Cases BW with $\varepsilon_1 = \varepsilon_2 = 1.006$, 1.008 and 1.01.

TABLE IX. Amplitudes of the wave components from the first order to the third order of the

Cases BW with $\varepsilon_1 = \varepsilon_2 = 1.006, 1.008, 1.01$; $\varepsilon_1 = 1.007, \varepsilon_2 = 1.008$ and $\varepsilon_1 = 1.0065, \varepsilon_2 = 1.008$

Amplitude (m)	$\varepsilon_1 (= \varepsilon_2)$			$\varepsilon_1 = 1.007$, $\varepsilon_2 = 1.008$	$\varepsilon_1 = 1.0065$, $\varepsilon_2 = 1.008$
	1.006	1.008	1.01		
$a(f_1)$	0.105687	0.113925	0.120801	0.129123	0.138147
$a(f_2)$	0.143485	0.154952	0.164024	0.144214	0.137890
$a(2f_1)$	0.002907	0.003627	0.003950	0.004442	0.004922
$a(2f_2)$	0.007326	0.009165	0.009710	0.008641	0.008029
$a(f_1 + f_2)$	0.007133	0.008508	0.009574	0.008875	0.009034
$a(f_1 - f_2)$	0.001206	0.001675	0.002460	0.001493	0.001472
$a(3f_1)$	0.000139	0.000212	0.000263	0.000284	0.000319
$a(3f_2)$	0.000738	0.001256	0.001849	0.000974	0.000876
$a(2f_1 + f_2)$	0.000432	0.000604	0.000753	0.000668	0.000710
$a(f_1 + 2f_2)$	0.000718	0.000992	0.001171	0.000985	0.000965
$a(2f_1 - f_2)$	0.009398	0.013054	0.012437	0.015433	0.016353
$a(f_1 - 2f_2)$	0.038920	0.054585	0.060127	0.048538	0.043462

B. Analyses based on $\varepsilon_1 \neq \varepsilon_2$

As shown in Table VIII, it can be seen that S_d approaches a relatively smaller value (0.013) in the case of $\varepsilon_1 = \varepsilon_2 = 1.008$, which represents that the case ($\varepsilon_1 = \varepsilon_2 = 1.008$) is much closer to the conservation state ($S_d = 0$) of the mean rates of the mass, momentum and energy fluxes before and after the interaction than other cases in Table VIII. Obviously, the above analysis is based on the assumption that ε_1 is equal to ε_2 for the steady-state bi-chromatic

wave field after the interaction. However, it is essential to consider $\varepsilon_1 \neq \varepsilon_2$ for the bi-chromatic wave field. Table X presents the values for S_d for the matrix of ε_1 and ε_2 ranging from 1.005 to 1.01 with an increment of 0.001. As shown in Table X, the minimum values for S_d in each row ($0.02,\ 0.010,\ 0.009,\ 0.013,\ 0.027,\ 0.034$) arises in the same column in which $\varepsilon_2 = 1.008$. For the column with $\varepsilon_2 = 1.008$, it is noted that the minimum value for S_d is 0.009 which is calculated in the case of $\varepsilon_1 = 1.007$ and $\varepsilon_2 = 1.008$. This indicates that $\varepsilon_1 \neq \varepsilon_2$ can yield a lower value for S_d compared to the cases in Table VIII which are based on the assumption that $\varepsilon_1 = \varepsilon_2$, e.g., there is a slight difference (0.004) for S_d in the case of $\varepsilon_1 = \varepsilon_2 = 1.008$ and $\varepsilon_1 = 1.007, \varepsilon_2 = 1.008$. It is worth noting that all the values for S_d presented in Table X are calculated based on the HAM solutions with a total averaged residual error at least 10^{-6} for each steady wave field.

TABLE X. The standard deviation S_d for the matrix of ε_1 and ε_2 with an increment of 0.001

S_d		ε_2					
		1.005	1.006	1.007	1.008	1.009	1.01
ε_1	1.005	0.229	0.150	0.070	0.020	0.098	-
	1.006	0.209	0.140	0.069	0.010	0.094	0.172
	1.007	0.193	0.132	0.061	0.009	0.087	0.167
	1.008	0.185	0.125	0.066	0.013	0.073	0.151
	1.009	0.105	0.121	0.067	0.027	0.082	0.130
	1.01	-	0.138	0.082	0.034	0.067	0.157

Table XI further presents the values for S_d for the matrix of ε_1 and ε_2 around $\varepsilon_1 = 1.007$ and $\varepsilon_2 = 1.008$ with a smaller increment of 0.0005. As shown in Table XI, similar

476 to the tendency in Table X, the minimum values for S_d in each row arise in the column with
477 $\varepsilon_2 = 1.008$. It is clear that compared to the case of $\varepsilon_1 = 1.007$ and $\varepsilon_2 = 1.008$, a smaller value
478 (0.007) for S_d can be obtained when $\varepsilon_1 = 1.0065$ and $\varepsilon_2 = 1.008$. This indicates that it is
479 possible to obtain much smaller values for S_d by subdividing around $\varepsilon_1 = 1.007$ and
480 $\varepsilon_2 = 1.008$ with a smaller increment. However, in this paper, the Case BW with $\varepsilon_1 = 1.0065$,
481 $\varepsilon_2 = 1.008$ and $S_d = 0.007$ is supposed to be highly close to the conservation state, thus it is
482 not essential to seek smaller values for S_d.
483
484 TABLE XI. The standard deviation S_d for the matrix of ε_1 and ε_2 with an increment of
485 0.0005

S_d		ε_2				
		1.007	1.0075	1.008	1.0085	1.009
ε_1	1.006	0.069	0.031	0.010	0.049	0.094
	1.0065	0.068	0.031	0.007	0.046	0.086
	1.007	0.061	0.032	0.009	0.044	0.087
	1.0075	0.066	0.034	0.012	0.041	0.078
	1.008	0.066	0.037	0.013	0.038	0.073

486
487 Fig. 10 shows the wave profiles at $t = 0$ for the Cases BW with $\varepsilon_1 = 1.0065$, $\varepsilon_2 = 1.008$,
488 $\varepsilon_1 = 1.007, \varepsilon_2 = 1.008$ and $\varepsilon_1 = \varepsilon_2 = 1.008$. In contrast to the characteristics in Fig. 8, it can be
489 seen in Fig. 10 that for the three bi-chromatic wave cases, no significant difference exists for
490 the profile of the largest wave crest at $x = 0$ and wave trough next to $x = 0$, whilst slight
491 difference arises between the wave crest and wave trough around $x = 30$. This indicates that
492 the slight difference for S_d between the three bi-chromatic wave cases does not lead to
493 remarkable influence on the wave profile. Fig. 11 shows the amplitude spectra of the

494 bi-chromatic wave Cases BW with $\varepsilon_1 = 1.0065$, $\varepsilon_2 = 1.008$ and $\varepsilon_1 = 1.007$, $\varepsilon_2 = 1.008$ It is
495 seen again that high-order nonlinear wave components are quite evident. It is also noted that
496 for the Case BW with $\varepsilon_1 = 1.007$, $\varepsilon_2 = 1.008$, the amplitude of the primary wave f_2 appears
497 to be slightly greater than that of the primary wave f_1; whilst for the Case BW with
498 $\varepsilon_1 = 1.0065$, $\varepsilon_2 = 1.008$, the amplitude of the primary wave f_2 appears to be identical to that
499 of the primary wave f_1. To further see the amplitudes of various order wave components, the
500 amplitudes of the wave components from the first order to the third order of the Cases BW
501 with $\varepsilon_1 = 1.007$, $\varepsilon_2 = 1.008$ and $\varepsilon_1 = 1.0065$, $\varepsilon_2 = 1.008$ are also presented in Table IX. It is
502 observed in Table IX that the amplitudes of various order wave components of the Cases BW
503 with $\varepsilon_1 = \varepsilon_2 = 1.008$, $\varepsilon_1 = 1.007$, $\varepsilon_2 = 1.008$ and $\varepsilon_1 = 1.0065$, $\varepsilon_2 = 1.008$ appear to be evidently
504 different. It is these differences that produce the discrepancy of the mean rates of the mass,
505 momentum and energy fluxes between these three cases. On the other hand, for the Case BW
506 with $\varepsilon_1 = 1.0065$ and $\varepsilon_2 = 1.008$, which leads to a smaller value (0.007) for S_d, the ratio of
507 the primary wave amplitudes ($a(f_1)/a(f_2) \approx 1.002$) tend to approach 1 compared to the Cases
508 BW with $\varepsilon_1 = 1.007$, $\varepsilon_2 = 1.008$ ($a(f_1)/a(f_2) \approx 0.895$) and $\varepsilon_1 = \varepsilon_2 = 1.008$ ($a(f_1)/a(f_2) \approx 0.735$).
509 This means that the energy of the primary waves tends to balance each other for the Case BW
510 which is much closer to the conservation state after the interaction.
511

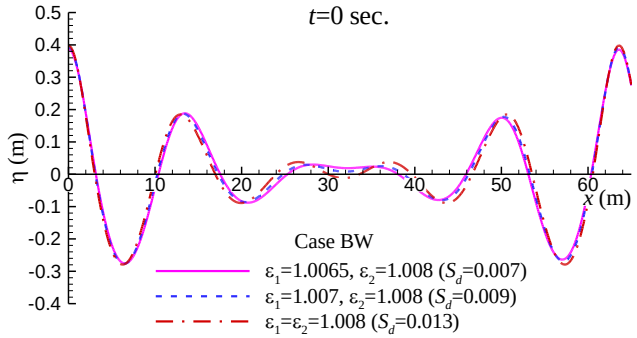

512

513 FIG. 10. Wave profile comparison for the Cases BW with $\varepsilon_1 = 1.0065$, $\varepsilon_2 = 1.008$; $\varepsilon_1 = 1.007$,

514 $\varepsilon_2 = 1.008$ and $\varepsilon_1 = \varepsilon_2 = 1.008$.

515

516

517

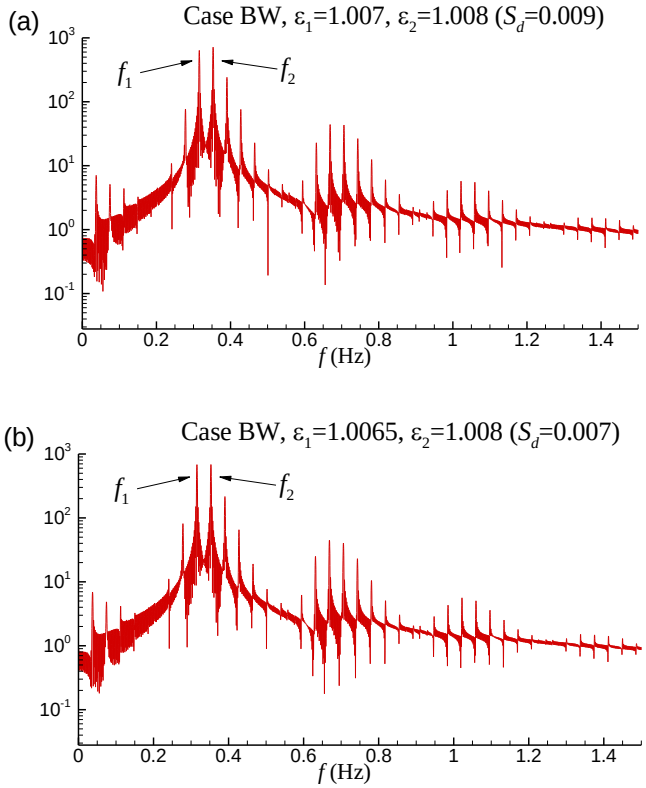

518

519

520 FIG. 11. Amplitude spectra for the Cases BW with $\varepsilon_1 = 1.007$, $\varepsilon_2 = 1.008$ and $\varepsilon_1 = 1.0065$,

521 $\varepsilon_2 = 1.008$.

Fig. 12 shows the amplitudes of the primary waves of the monochromatic wave Cases W1, W2, as well as the bi-chromatic wave Case BW with $\varepsilon_1 = 1.0065$ and $\varepsilon_2 = 1.008$. As shown in Fig. 12, the amplitudes of the primary waves of each nonlinear monochromatic wave train before the interaction are 0.157823 m and 0.126214 m, respectively, while the corresponding amplitudes of the primary waves of the bi-chromatic wave field with $\varepsilon_1 = 1.0065$ and $\varepsilon_2 = 1.008$ are 0.138147 m and 0.13789 m, respectively. The amplitude of the primary wave with a lower frequency (ω_1=1.98386 rad/s) drops from 0.157823 m to 0.138147 m with a decrement approximately 18.4%, while the one with a higher frequency (ω_2=2.21802 rad/s) increases from 0.126214 m to 0.13789 m with an increment approximately 14.3%. It is clear that the amplitude of the primary wave with a lower frequency tends to decrease; while the one with a higher frequency tends to increase in terms of $S_d = 0.007$ of the mean rates of the mass, momentum and energy fluxes before and after the interaction. This demonstrates the energy transfer from the primary wave with a lower frequency to that with a higher frequency during the interaction.

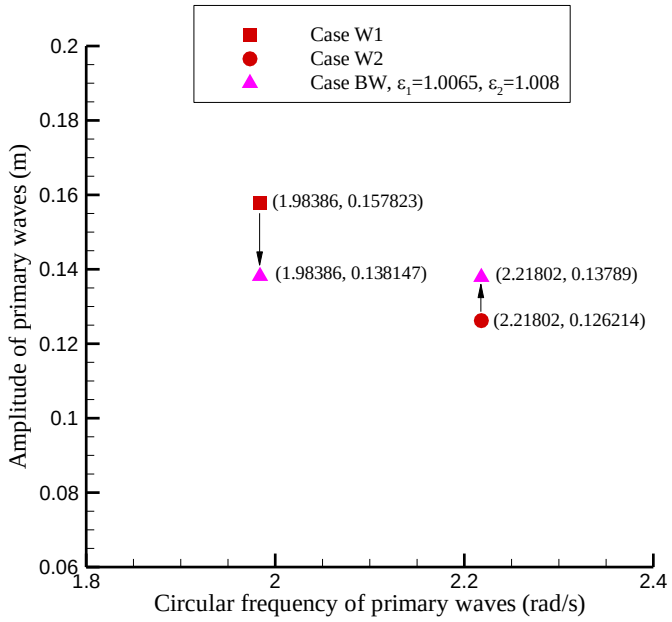

FIG. 12. Amplitudes of the primary waves of Cases W1, W2 and the Case BW with $\varepsilon_1 = 1.0065, \varepsilon_2 = 1.008$.

Fig. 13 shows the horizontal velocity profiles underneath the wave crest and wave trough for the monochromatic wave Cases W1, W2, and the bi-chromatic wave case with $\varepsilon_1 = 1.0065$ and $\varepsilon_2 = 1.008$ which is much closer to the conservation state. The profiles of the linear superposition of the velocity profiles for Cases W1 and W2 are also presented in Fig. 13. As shown in Fig. 13, for the bi-chromatic wave case, the largest horizontal velocity of the water particle on the largest wave trough (next to $x = 0$) is approximately 0.55 m/s which is almost identical to the linear superposition value (0.552 m/s) of the largest horizontal velocities on the wave trough of the two monochromatic wave Cases W1 and W2; whilst the largest horizontal velocity of the water particle on the largest wave crest (at $x = 0$) of the bi-chromatic wave case is approximately 0.898 m/s which is 1.43 times the linear superposition value (0.627 m/s) of the largest horizontal velocities on the wave crest of the two monochromatic wave Cases W1 and W2. It is also noted that for the Case BW with $\varepsilon_1 = 1.0065$, $\varepsilon_2 = 1.008$ and the linear superposition of Cases W1 and W2, the differences between the velocity profiles under the wave crests (Δu) gradually diminish as water depth deepens and tend to coincide with each other when the depth is deeper than $-d/5$ (i.e. -4 m); while the velocity profiles under the wave trough appear to coincide along the whole water depth. This evidently indicates that the nonlinear interaction between the two monochromatic waves leads to significant increases in the horizontal velocity of the water particles under the largest wave crest compared to the corresponding linear superposition values, especially close

559 to the free surface.

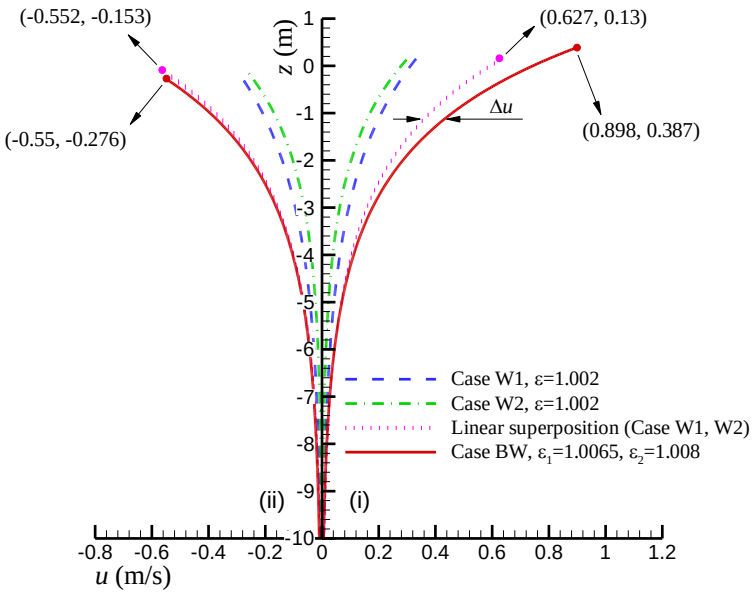

560

561 FIG. 13. Water particle horizontal velocity profiles at $t=0$: (i) under the wave crest at $x=0$;

562 (ii) under the wave trough next to $x=0$.

563

564 ## VI. CONCLUSIONS

565 Nonlinear progressive bi-chromatic waves in water of finite depth are studied by using

566 the homotopy analysis method. The equations for the mass, momentum and energy fluxes

567 based on accurate high-order homotopy series solutions are derived using the discrete

568 integrations and Fourier series-based fittings. The relationship between the steady-state

569 bi-chromatic wave field and the two nonlinear monochromatic wave trains is established in

570 terms of the conservation equations for the mean rates of the mass, momentum and energy

571 fluxes before and after the interaction. The parametric analysis on ε_1 and ε_2 of the

572 bi-chromatic wave field is performed to obtain sufficiently small values for the standard

573 deviation S_d, which is applied to describe the deviation from the conservation state ($S_d=0$)

574 before and after the interaction of the two nonlinear monochromatic wave trains. The
575 following conclusions are drawn from this study.

576 1. The discrete integration and the fitting based on the Fourier series can provide accurate
577 expressions for the mass, momentum and energy fluxes of a monochromatic wave field
578 as well as a steady-state bi-chromatic wave field.
579 2. Under the assumption either $\varepsilon_1 = \varepsilon_2$ or $\varepsilon_1 \neq \varepsilon_2$, some cases ($S_d \leq 0.013$) are found to be
580 very close to the conservation state ($S_d = 0$) of the mean rates of the mass, momentum
581 and energy fluxes before and after the interaction.
582 3. The amplitude of the primary wave with a lower frequency tends to decrease, and the
583 one with a higher frequency tends to increase based on the conservation analysis on the
584 mean rates of the mass, momentum and energy fluxes before and after the interaction.
585 4. The energy of the primary waves of the bi-chromatic wave Case BW which is much
586 closer to the conservation state ($S_d = 0$) after the interaction, tends to balance each other.
587 5. The nonlinear interaction between the two monochromatic waves is found to lead to
588 significant increases in the horizontal velocity of the water particles under the largest
589 wave crest, especially close to the free surface.

590

591 **ACKNOWLEDGMENTS**

592 The authors would like to express their gratitude to the National Natural Science
593 Foundation of China (Grant Nos. 51239007 and 51209136) and Newton Research
594 Collaboration Programme Award, The Royal Academy of Engineering UK for financial
595 support.

596

597 ## APPENDIX: SOLUTION PROCEDURE BY HAM

598 ### 1. *Zero*th-order deformation equation

599 In the framework of HAM, there is great freedom to choose the linear auxiliary operator.

600 According to the linear part of the nonlinear boundary conditions (10) and (11), two linear

601 auxiliary operators are chosen as

602 $$L_1\left[(\cdot)\right]=(\cdot), \tag{A1}$$

603 $$L_2\left[\phi\right]=\bar{\omega}_1{}^2\frac{\partial^2\phi}{\partial\theta_1{}^2}+2\bar{\omega}_1\bar{\omega}_2\frac{\partial^2\phi}{\partial\theta_1\partial\theta_2}+\bar{\omega}_2{}^2\frac{\partial^2\phi}{\partial\theta_2{}^2}+g\frac{\partial\phi}{\partial z}, \tag{A2}$$

604 where

605 $$\bar{\omega}_i=\sqrt{gk_i\tanh\left(k_id\right)}\ (i=1,2). \tag{A3}$$

606 Based on the nonlinear boundary conditions, two nonlinear operators can be defined as

607 $$N_1\left[\eta,\phi\right]=\eta-\frac{1}{g}(\omega_1\frac{\partial\phi}{\partial\theta_1}+\omega_2\frac{\partial\phi}{\partial\theta_2}-f), \tag{A4}$$

608 $$\begin{aligned}N_2\left[\phi\right]=&\omega_1^2\frac{\partial^2\phi}{\partial\theta_1^2}+2\omega_1\omega_2\frac{\partial^2\phi}{\partial\theta_1\partial\theta_2}+\omega_2^2\frac{\partial^2\phi}{\partial\theta_2^2}+g\frac{\partial\phi}{\partial z}\\&-2(\omega_1\frac{\partial f}{\partial\theta_1}+\omega_2\frac{\partial f}{\partial\theta_2})+\hat{\nabla}\phi\cdot\hat{\nabla}f.\end{aligned} \tag{A5}$$

609 Then the *zero*th-order deformation equation can be constructed as

610 $$\hat{\nabla}^2\breve{\phi}\left(\theta_1,\theta_2,z;q\right)=0,\qquad -d<z\le\breve{\eta}(\theta_1,\theta_2;q), \tag{A6}$$

611 which is subject to the bottom boundary condition:

612 $$\frac{\partial\breve{\phi}\left(\theta_1,\theta_2,z;q\right)}{\partial z}=0,\qquad z=-d, \tag{A7}$$

613 and two nonlinear boundary conditions on $z=\breve{\eta}(\theta_1,\theta_2;q)$ are:

614 $$\left(1-q\right)L_1\left[\breve{\eta}(\theta_1,\theta_2;q)\right]=qc_0N_1\left[\breve{\eta}(\theta_1,\theta_2;q),\breve{\phi}\left(\theta_1,\theta_2,z;q\right)\right], \tag{A8}$$

615 $$\left(1-q\right)L_2\left[\breve{\phi}(\theta_1,\theta_2,z;q)-\phi_0(\theta_1,\theta_2,z)\right]=qc_0N_2\left[\breve{\phi}(\theta_1,\theta_2,z;q)\right], \tag{A9}$$

where $q \in [0,1]$ is an embedding parameter; c_0 is the so-called nonzero convergence-control parameter; $\phi_0(\theta_1,\theta_2,z)$ is the initial estimate of the potential function; and $\breve{\phi}(\theta_1,\theta_2,z;q)$ and $\breve{\eta}(\theta_1,\theta_2;q)$ are the mapping functions, respectively.

When $q=0$, the *zero*th-order deformation Eqs. (A6)-(A9) have the solution:

$$\breve{\phi}(\theta_1,\theta_2,z;0)=\phi_0(\theta_1,\theta_2,z), \tag{A10}$$

$$\breve{\eta}(\theta_1,\theta_2;0)=0. \tag{A11}$$

When $q=1$, the *zero*th-order deformation Eqs. (A6)-(A9) are equivalent to the original Partial Differential Equations (PDEs) (8)-(11), respectively, provided that:

$$\breve{\phi}(\theta_1,\theta_2,z;1)=\phi(\theta_1,\theta_2,z), \tag{A12}$$

$$\breve{\eta}(\theta_1,\theta_2;1)=\eta(\theta_1,\theta_2). \tag{A13}$$

Thus, as the embedding parameter q increases from 0 to 1, $\breve{\phi}(\theta_1,\theta_2,z;q)$ and $\breve{\eta}(\theta_1,\theta_2;q)$ deform continuously from initial estimates $\phi_0(\theta_1,\theta_2,z)$ and 0 to become the exact solutions of the original problem, respectively.

The Maclaurin series of $\breve{\phi}(\theta_1,\theta_2,z;q)$ and $\breve{\eta}(\theta_1,\theta_2;q)$, with respect to the embedding parameter q, can be expressed as

$$\breve{\phi}(\theta_1,\theta_2,z;q)=\sum_{m=0}^{+\infty}\phi_m(\theta_1,\theta_2,z)q^m, \tag{A14}$$

$$\breve{\eta}(\theta_1,\theta_2;q)=\sum_{m=0}^{+\infty}\eta_m(\theta_1,\theta_2)q^m, \tag{A15}$$

where

$$\phi_m(\theta_1,\theta_2,z)=\frac{1}{m!}\frac{\partial^m\breve{\phi}(\theta_1,\theta_2,z;q)}{\partial q^m}\bigg|_{q=0}, \tag{A16}$$

$$\eta_m(\theta_1,\theta_2)=\frac{1}{m!}\frac{\partial^m\breve{\eta}(\theta_1,\theta_2;q)}{\partial q^m}\bigg|_{q=0}. \tag{A17}$$

Assuming that c_0 is properly chosen so that the Maclaurin series (A14) and (A15) converge at $q=1$, then the so-called homotopy-series solutions are obtained as

$$\phi(\theta_1,\theta_2,z)=\phi_0(\theta_1,\theta_2,z)+\sum_{m=1}^{+\infty}\phi_m(\theta_1,\theta_2,z), \tag{A18}$$

$$\eta(\theta_1,\theta_2)=\sum_{m=1}^{+\infty}\eta_m(\theta_1,\theta_2). \tag{A19}$$

2. High-order deformation equation

Substituting the series in Eqs. (A14) and (A15) into the *zero*th-order deformation equations and equating the like-power of q, the so-called *m*th-order deformation equations are

$$\hat{\nabla}^2\phi_m(\theta_1,\theta_2,z)=0, \tag{A20}$$

$$\frac{\partial\phi_m(\theta_1,\theta_2,z;q)}{\partial z}=0,\quad z=-d, \tag{A21}$$

$$\bar{L}_2\left[\phi_m\left(\theta_1,\theta_2,z\right)\right]=R_m^{\phi}(\theta_1,\theta_2;c_0), \tag{A22}$$

$$\eta_m\left(\theta_1,\theta_2\right)=R_m^{\eta}(\theta_1,\theta_2;c_0), \tag{A23}$$

where

$$R_m^{\phi}(\theta_1,\theta_2;c_0)=c_0\Delta_{m-1}^{\phi}+\chi_m S_{m-1}-\bar{S}_m, \tag{A24}$$

$$R_m^{\eta}(\theta_1,\theta_2;c_0)=c_0\Delta_{m-1}^{\eta}+\chi_m\eta_{m-1}, \tag{A25}$$

$$\Delta_m^{\phi}=\omega_1^2\bar{\phi}_m^{2,0}+2\omega_1\omega_2\bar{\phi}_m^{1,1}+\omega_2^2\bar{\phi}_m^{0,2}+g\bar{\phi}_{z,m}^{0,0}-2(\omega_1\Gamma_{m,1}+\omega_2\Gamma_{m,2})+\Lambda_m, \tag{A26}$$

$$\Delta_m^{\eta}=\eta_m-\frac{1}{g}(\omega_1\bar{\phi}_m^{1,0}+\omega_2\bar{\phi}_m^{0,1}-\Gamma_{m,0}), \tag{A27}$$

$\bar{L}_2[\phi]=L_2[\phi]\big|_{z=0}$ and $m\geq 1$. The definitions of S_m, $\bar{S}_m$, χ_m, Λ_m, $\bar{\phi}_{z,m}^{0,0}$, $\Gamma_{m,i}$, $\bar{\phi}_m^{i,j}$ $(i,j=0,1,2)$ and their detailed derivations can be found in Liao[15].

3. The initial estimate

Liao[12] has demonstrated that there is great freedom to choose the initial estimate in

657 HAM. The auxiliary linear operator in Eq. (A2) has the property:

658 $$\bar{L}_2[\Psi_{m,n}] = \lambda_{m,n} \cdot \sin\left(m\theta_1 + n\theta_2\right), \tag{A28}$$

659 where $\Psi_{m,n}$ is defined by Eq. (16) and

660 $$\lambda_{m,n} = g\left|mk_1 + nk_2\right| \tanh(\left|mk_1 + nk_2\right| d) - (m\bar{\omega}_1 + n\bar{\omega}_2)^2. \tag{A29}$$

661 Therefore, the inverse operator $\bar{L}_2^{-1}$ is defined as

662 $$\bar{L}_2^{-1}\left[\sin\left(m\theta_1 + n\theta_2\right)\right] = \frac{\Psi_{m,n}}{\lambda_{m,n}}, \qquad \lambda_{m,n} \neq 0. \tag{A30}$$

663 Note that the inverse operator $\bar{L}_2^{-1}$ has definition only for non-zero values of $\lambda_{m,n}$. When

664 $\lambda_{m,n} = 0$,

665 $$g\left|mk_1 + nk_2\right| \tanh\left(\left|mk_1 + nk_2\right| d\right) = (m\bar{\omega}_1 + n\bar{\omega}_2)^2. \tag{A31}$$

666 In this paper, there are only $\lambda_{1,0} = 0$ and $\lambda_{0,1} = 0$. Thus, an initial estimate for $\phi_0(\theta_1, \theta_2, z)$

667 can be chosen as

668 $$\phi_0\left(\theta_1, \theta_2, z\right) = b_{1,0} \cdot \Psi_{1,0}\left(\theta_1, \theta_2, z\right) + b_{0,1} \cdot \Psi_{0,1}\left(\theta_1, \theta_2, z\right), \tag{A32}$$

669 where $b_{1,0}$ and $b_{0,1}$ are unknown constants to be determined later.

670 ## 4. Solution procedure

671 Considering the rule for solution expressions (14) and (15) and the property of the

672 auxiliary linear operator L_2 in Eq. (A28), the right-hand side of Eq. (A22) can be expressed

673 as

674 $$R_m^{\phi} = \tilde{b}_{m,1,0} \sin\theta_1 + \tilde{b}_{m,0,1} \sin\theta_2 + \sum_{i=0}^{I_m} \sum_{\substack{j=-J_m \\ i+j\neq 1}}^{J_m} \tilde{b}_{m,i,j} \sin\left(i\theta_1 + j\theta_2\right), \tag{A33}$$

675 where $\tilde{b}_{m,i,j}$ are coefficients and (I_m, J_m) is related to the right-hand side of Eq. (A22).

676 According to the property of the auxiliary linear operator L_2,

677 $$\begin{cases} \tilde{b}_{m,1,0} = 0, \\ \tilde{b}_{m,0,1} = 0 \end{cases} \tag{A34}$$

678 have to be enforced to avoid the so-called secular terms. Therefore, using Eq. (A31), it is

679 convenient to obtain the solution of Eq. (A22):

680 $$\phi_m(\theta_1,\theta_2,z) = \sum_{i=0}^{I_m} \sum_{\substack{j=-J_m \\ i+j\neq 1}}^{J_m} \bar{b}_{m,i,j} \Psi_{m,n}(\theta_1,\theta_2,z) + \bar{b}_{m,1,0}\Psi_{1,0}(\theta_1,\theta_2,z) + \bar{b}_{m,0,1}\Psi_{0,1}(\theta_1,\theta_2,z), \tag{A35}$$

681 where $\bar{b}_{m,1,0}$ and $\bar{b}_{m,0,1}$ are unknown coefficients to be determined in the $(m+1)\text{th}-$order

682 deformation equation.

683 When $m=1$ using Eq. (A34), the unknown coefficients $b_{1,0}$ and $b_{0,1}$ in Eq. (A32) can be

684 obtained for the initial estimate $\phi_0(\theta_1,\theta_2,z)$. Substituting the $\phi_0(\theta_1,\theta_2,z)$ into the Eq.

685 (A23), the $\eta_1(\theta_1,\theta_2)$ can be directly obtained.

686 When $m\geq 2$, the unknown coefficients $\bar{b}_{m-1,1,0}$ and $\bar{b}_{m-1,0,1}$ in Eq. (A35) can also be obtained

687 by using the Eq. (A34). As long as $\bar{b}_{m-1,1,0}$ and $\bar{b}_{m-1,0,1}$ are known, $\eta_m(\theta_1,\theta_2)$ and

688 $\phi_m(\theta_1,\theta_2,z)$ can be obtained in a similar way. All of this can be done successively and

689 efficiently by means of the symbolic computation software-*Mathematica* 7. At the $M\text{th}-$

690 order approximations, there are

691 $$\begin{cases} \phi(\theta_1,\theta_2,z) \approx \phi_0(\theta_1,\theta_2,z) + \sum_{m=1}^{M} \phi_m(\theta_1,\theta_2,z), \\ \eta(\theta_1,\theta_2) \approx \sum_{m=1}^{M} \eta_m(\theta_1,\theta_2). \end{cases} \tag{A36}$$

692 ## 5. Optimal convergence-control parameters

693 For the $m\text{th}-$order approximations $\phi(\theta_1,\theta_2,z)$ and $\eta(\theta_1,\theta_2)$, there is still one

694 unknown parameter c_0, which is used to guarantee the convergence of the approximation

695 series. In order to choose an optimal c_0, two averaged residual square errors of the boundary

696 conditions are defined as

$$E_m^{\phi} = \frac{1}{(1+I_k)}\frac{1}{(1+J_k)}\sum_{i=0}^{I_k}\sum_{j=0}^{J_k}\left(N_1\left[\phi(\theta_1,\theta_2,z)\right]\Big|_{\theta_1=i\Delta\theta_1,\ \theta_2=j\Delta\theta_2}\right)^2, \tag{A37}$$

$$E_m^{\eta} = \frac{1}{(1+I_k)}\frac{1}{(1+J_k)}\sum_{i=0}^{I_k}\sum_{j=0}^{J_k}\left(N_2\left[\phi(\theta_1,\theta_2,z),\ \eta(\theta_1,\theta_2)\right]\Big|_{\theta_1=i\Delta\theta_1,\ \theta_2=j\Delta\theta_2}\right)^2, \tag{A38}$$

where I_k and J_k are the numbers of discrete points, $\Delta\theta_1 = \pi / I_k$ and $\Delta\theta_2 = \pi / J_k$. In the present work, $I_k = J_k = 20$ is chosen based on the sensitivity test without loss of generality. Defining the total averaged residual square error as $E_m^T = E_m^{\phi} + E_m^{\eta}$, then by solving $\mathrm{d}E_m^T / \mathrm{d}c_0 = 0$, the optimal value of c_0 can be obtained, which corresponds to the minimum value of E_m^T.

REFERENCES

[1]O. M. Phillips, "On the dynamics of unsteady gravity waves of finite amplitude Part 1. The elementary interactions," J. Fluid Mech. **9**, 193 (1960).

[2]M. S. Longuet-Higgins, "Resonant interactions between two trains of gravity waves," J. Fluid Mech. **12**, 321 (1962).

[3]W. J. Pierson, "Oscillatory third-order perturbation solutions for sums of interacting long-crested Stokes waves on deep water," J. Ship Res. **37**, 354 (1993).

[4]J. F. Dalzell, "A note on finite depth second-order wave–wave interactions," Appl. Ocean Res. **21**, 105 (1999).

[5]T. Ohyama, D.-S. Jeng, and J. R. C. Hsu, "Fourth-order theory for multiple-wave interaction," Coastal Eng. **25**, 43 (1995).

[6]L. Chen, and J. Zhang, "On interaction between intermediate-depth long waves and deep-water short waves," Ocean Eng. **25**, 395 (1998).

[7]J. Zhang, and L. Chen, "General third-order solutions for irregular waves in deep water," J. Eng. Mech. **125**, 768 (1999).

[8]P. A. Madsen, and D. R. Fuhrman, "Third-order theory for bichromatic bi-directional water waves," J. Fluid Mech. **557**, 369 (2006).

[9]T. S. Jang, and S. H. Kwon, "Application of nonlinear iteration scheme to the nonlinear water wave problem: Stokian wave," Ocean Eng. **32**, 1864 (2005).

[10]T. S. Jang, S. H. Kwon, and H. S. Choi, "Nonlinear wave profiles of wave–wave interaction in a finite water depth by fixed point approach," Ocean Eng. **34**, 451 (2007).

[11]Z. Lin, L. Tao, Y. C. Pu, and A. J. Murphy, "Fully nonlinear solution of bi-chromatic

deep-water waves," Ocean Eng. **91**, 290 (2014).

[12]S. Liao, *Beyond perturbation: introduction to the homotopy analysis method* (Chapman and Hall, London/CRC, Boca Raton, FL, 2003).

[13]S. Liao, and K. Cheung, "Homotopy analysis of nonlinear progressive waves in deep water," J. Eng. Math. **45**, 105 (2003).

[14]L. Tao, H. Song, and S. Chakrabarti, "Nonlinear progressive waves in water of finite depth — an analytic approximation," Coastal Eng. **54**, 825 (2007).

[15]S. Liao, "On the homotopy multiple-variable method and its applications in the interactions of nonlinear gravity waves," Commun. Nonlinear Sci. and Numer. Simul. **16**, 1274 (2011).

[16]D. Xu, Z. Lin, S. Liao, and M. Stiassnie, "On the steady-state fully resonant progressive waves in water of finite depth," J. Fluid Mech. **710**, 379 (2012).

[17]Z. Liu, and S. Liao, "Steady-state resonance of multiple wave interactions in deep water," J. Fluid Mech. **742**, 664 (2014).

18A. D. D. Craik, *Wave interactions and fluid flows* (Cambridge University Press, Cambridge, 1985)

[19]R. E. Baddour, and S. W. Song, "Interaction of higher-order water waves with uniform currents," Ocean Eng. **17**, 551 (1990).

[20]R. E. Baddour, and S. Song, "On the interaction between waves and currents," Ocean Eng. **17**, 1 (1990).

[21]M. Hasanat Zaman, and E. Baddour, "Interaction of waves with non-colinear currents," Ocean Eng. **38**, 541 (2011).

[22]Y. Ma, G. Dong, and X. Ma, "Separation of low frequency waves by an analytical method,"

749 Proceedings of the 32th international conference on coastal engineering (ICCE), ASCE,
750 Shanghai, (2010).
751 [23]G. B. Whitham, “Mass, momentum and energy flux in water waves,” J. Fluid Mech. **12**, 135
752 (1962).